RESEARCH PAPER

Encapsulation of Gold Nanoparticles into Functionalized Silica Nanoparticles Stabilized on Triacetyl Cellulose for Gluten Determination

Fatemeh Sadat Mousavizadeh and Nahid Sarlak *

Department of Chemistry, Faculty of Science, Lorestan University, Khorramabad, Iran

ARTICLE INFO

ABSTRACT

A sensitive, rapid, and portable optical sensor for the determination of gluten is fabricated. The sensing probe is composed of gold nanoparticles encapsulated into hyper branched polycitric acid modified silica nanoparticles Si-g-PCA/AuNPs. Portability is imposed by stabilizing the as-prepared sensing probe on the triacetyl cellulose membrane as a solid substrate. The sensing probe's synthesis and immobilization were thoroughly investigated by using spectroscopy and microscopy techniques including FT-IR, UV-vis, SEM, EDX, AFM, and BET analysis. The as-prepared sensor showed an increment at 530 nm in the presence of various concentrations of gluten. Effective parameters, including pH and response time on the sensor response, are precisely optimized, and a linear range from 49.50 to 370.37 μgmL^{-1} is obtained for gluten determination. The present sensor was successfully applied for gluten detection into gluten-free bread as a real sample. Moreover, the sensor showed multi-usage capability in which sensing characteristics could be recovered in the presence of 55% ethanol.

INTRODUCTION

The wheat proteins are classified into two groups, gliadins and glutenins, and they are called glutens. The elasticity of gluten proteins is because of glutenins. They are included low molecular weight (LMW) and high-molecular-weight (HMW) glutenins [1]. Gluten monomer sections are gliadins and cause the viscosity of gluten proteins that gliadins are dissolved in aqueous alcohols [2]. The combination and amount of gliadin and glutenin proteins are essential to wheat quality. Total proteins of wheat grains include about 50 % gliadins and 35 % glutenins [3]. Gliadin as the first subfraction of gluten protein was studied in the early 19th century, Its extraction and purification were relatively more straightforward than the other glutenin subfractions [4, 5]. Wheat gluten, the by-product protein of wheat starch, is considered as a substitute protein to replace expensive animal proteins due to its individual characteristics and inexpensive [6]. Also, due to the widespread use of gluten in the pharmaceutical and cosmetic food industries as a flavor enhancer, thickener, emulsifier, filler, and fortification ingredient, there are hidden sources of gluten in the daily diet [7].

One of the most important global issues is food safety, attracting extensive concern. Celiac disease (CD) is a chronic autoimmune illness in genetically susceptible persons, and it mainly arises from gliadin proteins [8]. Chronic diarrhea, weight loss, and abdominal distention (in 40–50% of patients) are common symptoms of celiac

* *Corresponding Author Email: sarlak.n@lu.ac.ir*

disease [8-10]. Since 2004, the rapid development of nanotechnology has offered a consequence completion that nanosensors prospects to satisfy applications in healthcare, homeland security, and other critical fields because of the availability of all methods of nanomaterials and improved nanofabrication approaches, combined with a greater understanding of nanoscales [11]. Advances in the age of nanotechnology are moving towards the fabrication of nanosensors that are flexible, specific, versatile, and sensitive. The objective of nanosensors is to screen and measure any chemical, mechanical and physical changes related to a marker of interest [12].

The extract of gliadin proteins is harrowing from wheat flour because of its complex mixture of proteins. For that reason, the development of a test that can correctly quantify gliadin content in food is a challenge [2]. Recently, various procedures are employed to study and measure gluten polypeptides, including high performance liquid chromatography [13-15], mass spectrometry [16], one-dimensional electrophoresis [17-22], two-dimensional electrophoresis [23-25], PCR [26] and some immunoassay-based platforms. The following are examples of the last two methods.

There are two main methods for the fabrication of gluten sensors: using the allergenic proteins or their peptide fragments and identify specific DNA sequences of the carrier cereals. Some of the sensors that have developed to detect and determine gluten so far based on these methods is listed as follow: an electrochemical sensor was designed based on aptamer targeting the gliadin immunodominant peptide 33-mer that triggers coeliac disease. The sensing layer created by adsorption of streptavidin and subsequent peptide immobilization on the surface of a screen-printed carbon electrode (SPCE). A competition between the peptide and gluten proteins from samples for a defined biotinylated aptamer concentration is recognized [27]. In another study, a microfluidic ELISA platform was combined with a custom-designed optical sensor to determine wheat gluten proteins [28]. An electrochemical biosensor was reported for gluten detection in food samples by chronoamperometry. In this research, the carbon electrode was modified with electrodeposition of the Protease enzyme with fullerene nanoparticles [29]. A label-free gliadin immunosensor was developed based on changes in the frequency of a quartz crystal microbalance (QCM) chip. They

obtained a higher sensitivity by using 25 nm AuNP-modified with chicken anti-gliadin antibodies (IgY) to a bare QCM electrode [30]. An electrochemical genosensor that expresses the gluten value in real samples by detecting DNA concentration or DNA copies was developed. PCR amplification was combined with genosensor for more sensitivity. Electrochemical genosensors are fabricated as alternative systems to detect DNA. They react with a hybridization recognition between two extra DNA strands: the target and probe element [31]. In another try for gluten study, a real-time PCR assay precisely detects the DNA to illustrate the presence of gluten from the cereals wheat, barley, and rye in foods [32]. In a research, an epitope chemical sensor was designed with a molecularly imprinted polymer (MIP) device to determine an immunogenic gluten octamer epitope [33]. Most of these sensors are expensive and require instruments and people with special skills to determine the amount of gluten in food samples, although they have good selectivity and sensitivity.

An ideal sensor should be small, selective, inexpensive to produce, short response time, and customer-friendly to be used without time-consuming or complex calibration or setup [34]. Optical chemical sensors are beneficial devices for monitoring analyte concentration within a sample matrix. They have many advantages such as small size, the feasibility of miniaturization, without electrical interference, inexpensive, safety, the possibility of remote sensing; simple production, reasonable sensitivity, and selectivity have been recognized [35]. Gluten sensors provided in the articles are complicated and expensive to produce.

In this work, gold nanocomposites (Si-g-PCA/Au) was synthesized and immobilized on the surface of triacetyl cellulose membrane to fabricate an optical nanosensor for gluten detection and determination. The kinetic absorption profiles of membranes were monitored by measuring the increase of nanosensor absorption at 530 nm, in the time range of 0–60 s after initiation of the reaction with 1 s intervals. An untrained operator without complex analysis devices can use the fabricated nanosensor for real sample determination.

MATERIALS AND METHODS
Instrumentation
Field emission scanning electron microscopy

(FE-SEM, Mira3 Tescan, Czech Republic), equipped with energy-dispersive X-ray spectroscopy (EDX, Mira3 Tescan, Czech Republic), was used to observe nanocomposite and nanosensor morphologies. Bio Atomic Force Microscope (AFM, Ara-research, Iran) was used to investigate the topography and morphology of the samples as well as the roughness of the samples. Infrared spectrums were obtained from Shimadzu FT-IR 160 spectrophotometer (Japan) using KBr pellets. A BET surface analyzer (BEL, BELSORP MINI II) was used to measure nitrogen adsorption-desorption isotherm at 77 K, while before the measurement, the samples were degassed using BEL PREP VAC II at 353 K for 2 h. The BET surface area, total pore volume, and micropore area were obtained from the adsorption isotherms. A Shimadzu Uv-Visible spectrophotometer (model UV-1800) with 1-cm glass cells was used for recording the absorption spectra measurements.

Reagents

All of the solvents (ammonia, ethanol, tetrahydrofuran (THF), ethylenediamine, tetrachloroauric (III) acid trihydrate (HAuCl$_4$ .3 H$_2$O) 99.5%, SiO$_2$ nanoparticles powder (15- 20 nm diameter), sodium chloride, Citric Acid-Monohydrate (code: 100242) and other materials were obtained from Merck company.

Preparation of sensing phase

Synthesize of Si-g-PCA/Au: Silica nanoparticles functionalized and polymerized with poly citric acid according to the reported procedure in the literature [36]. In brief, the 0.050 g of Silica nanoparticles were transferred to a polymerization ampule, 2.5 g of citric acid was added, and were sealed under vacuum. The mixture was heated from 120 ° C to 160 ° C while stirring for 3 hours. The obtained nanocomposite (Si-g-PCA) was dissolved in THF, then filtered, and was allowed to evaporate the solvent at room temperature.

An aqueous solution of Si-g-PCA nanocomposites and HAuCl$_4$ with a ratio of 1: 0.2 was prepared and its pH was adjusted to 5.5. Then the mixture ultrasonicated for 25 minutes and stirred for 240 minutes at room temperature until the solution color turned ruby red.

Immobilization of Si-g-PCA/Au

Triacetyl cellulose membrane surface applied as a nanosensor substrate. The waste photographic film tapes treated with commercial sodium hypochlorite for several seconds and removed colored gelatinous layers. The clean membrane prepared with the size of 4×1 cm and put in ethylene diamine for less than 3 minutes, and then it was washed with distilled water for removing the extra ethylene diamine. Next, it was placed in gold nanocomposites solution for 24 hours at ambient temperature. The nanosensor was rinsed with distilled water and stored underwater when not in use.

Gluten sample preparation

The chicken food powder was prepared from "Ard Azin" in Isfahan, Iran. The powder was sent to the Kermanshah Standard Office to determine the amounts of gliadin and glutenin. The results are shown in Table 1. The gliadin solution was prepared using the following method and used as a stock gluten source during measurements.

50 g gluten powder with 250 ml dimethyl chloride was stirred for 30 min at room temperature to prepare defatted gluten powder. The grout was then filtered, and the residue was placed under the frame hood for evaporating the remained solvent.

37.5 g of gluten powder was dispersed in 150 mL of 0.4 M NaCl solution at room temperature and was shaken for 30 min. This process was repeated until the solution did not change the

Table 1. The results of gluten powder analysis.

Proteins	79%	Gliadins	44.6%
		Glutenins	55.4%
Starch		20%	
Other compounds		1%	
Water absorption		100%	

color of Potassium Iodide to remove starch and the flour metabolic proteins, which are not contained in the gluten structure. Then it was centrifuged for 10 minutes at 6000 rpm at 20 ºC. The supernatants were discarded, and the pellet was manually re-suspended three times in 200 mL of a 55% ethanol-water solution to solute gluten proteins. The dispersed solution was stirred and centrifuged. The 55% ethanol-water solution contains both gliadins and glutenins. Gliadins and glutenins are separated by phase separation at low temperatures. A solution enriched in gliadin (up to 82%) was achieved from the solution after one night of resting at 4 ºC and centrifugation at 2 °C for 10 minutes at 20000 rpm. The sediment was primarily involved in glutenin and was discarded. The ethanol-water solution enriched in gliadin was freeze-dried. The powder was stored in the refrigerator when it was out of use. Since

gluten extraction was accomplished with wheat gluten powder that its fat, starch, and metabolic proteins have been removed, ethanol-water 55% is the main procedure to gluten extraction, and glutenins were separated by phase separation at low temperatures, the residual solid contains more than 90% gliadins. The obtained powder was used to prepare a 55% ethanol-water gluten stock solution [37].

The Procedure

The appropriate concentration of the gluten solution (1.19 – 370.37 µgmL^{-1}) was transferred to a glass cell; then, the prepared nanosensor was fixed within a cuvette using a particular frame. The absorption kinetics profile of the reaction between immobilized Si-g-PCA/Au and gluten proteins was recorded at 530 nm.
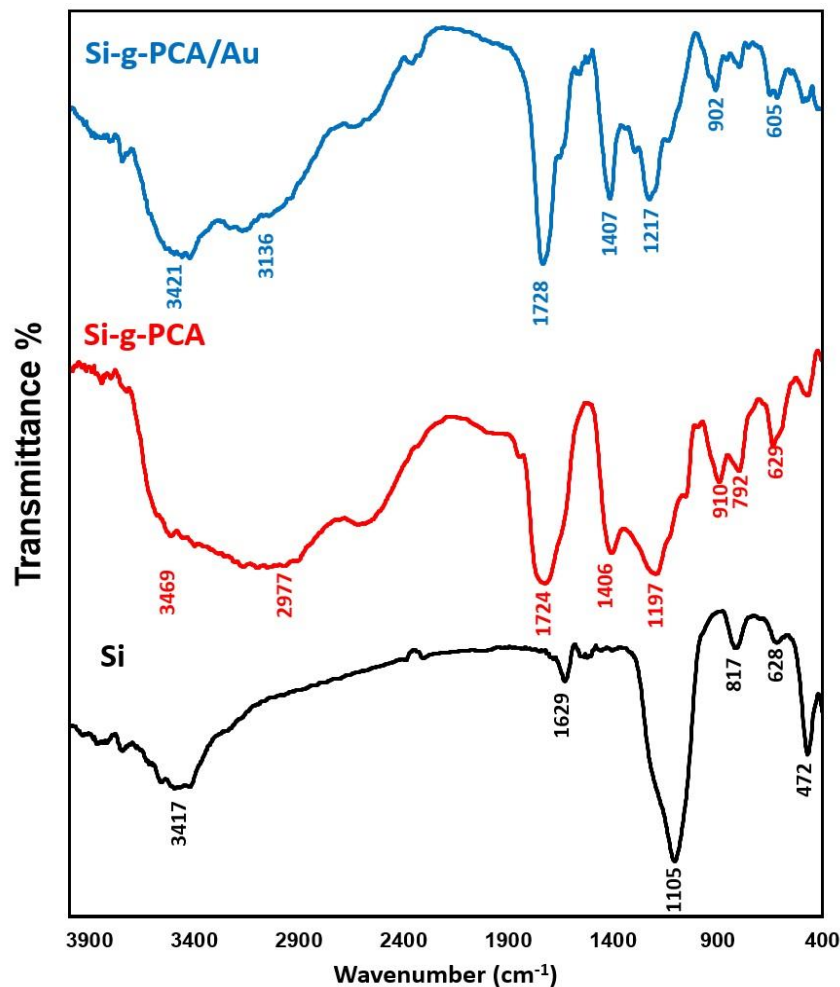

Fig. 1. FT-IR spectra of Si, Si-g-PCA, and Si-g-PCA/Au

RESULTS AND DISCUSSION

The FT-IR spectrum of silica NPs, Si-g-PCA, and Si-g-PCA/Au nanocomposites is shown in Fig. 1. The FTIR spectra of the silica nanoparticles illustrate the absorption band's asymmetric vibration of Si-O-Si at 1105 cm^{-1}, asymmetric vibration of Si-OH at 817 cm^{-1}, and symmetric vibration of Si-O at 628 cm^{-1}. The absorption bands at 1629 and 3417 cm^{-1}, were respectively allocated to the bending and stretching vibrations of the -OH bond from Si-OH and residual water.

In the FT-IR spectra of Si-g-PCA, the broadband at 2700-3600 cm^{-1} shows the presence of the acidic functional groups because of polymerized citric acid chains. Also, the band at 1724 cm^{-1} arising from carbonyl groups and the two bands at 1197 and 1406 cm^{-1} indicate the existence of C-O bonds and C=C bonds, respectively. The epoxy adsorption band was removed here due to polymerization processes. While the absorption bands of asymmetric and symmetric vibration of Si-O are still visible.

The FT-IR Spectra of Si-g-PCA/Au shows the decrease in intensity and width in the acidic functional groups and the asymmetric and symmetric Si-O vibration because of encapsulated gold nanoparticles in citric acid chains. Also, the decrease in the intensity of C-O bonds and C=C bonds absorption and the displacement absorption of C-O bonds from 1197 to 1217 cm^{-1} result from encapsulated gold nanoparticles in the citric acid chains.

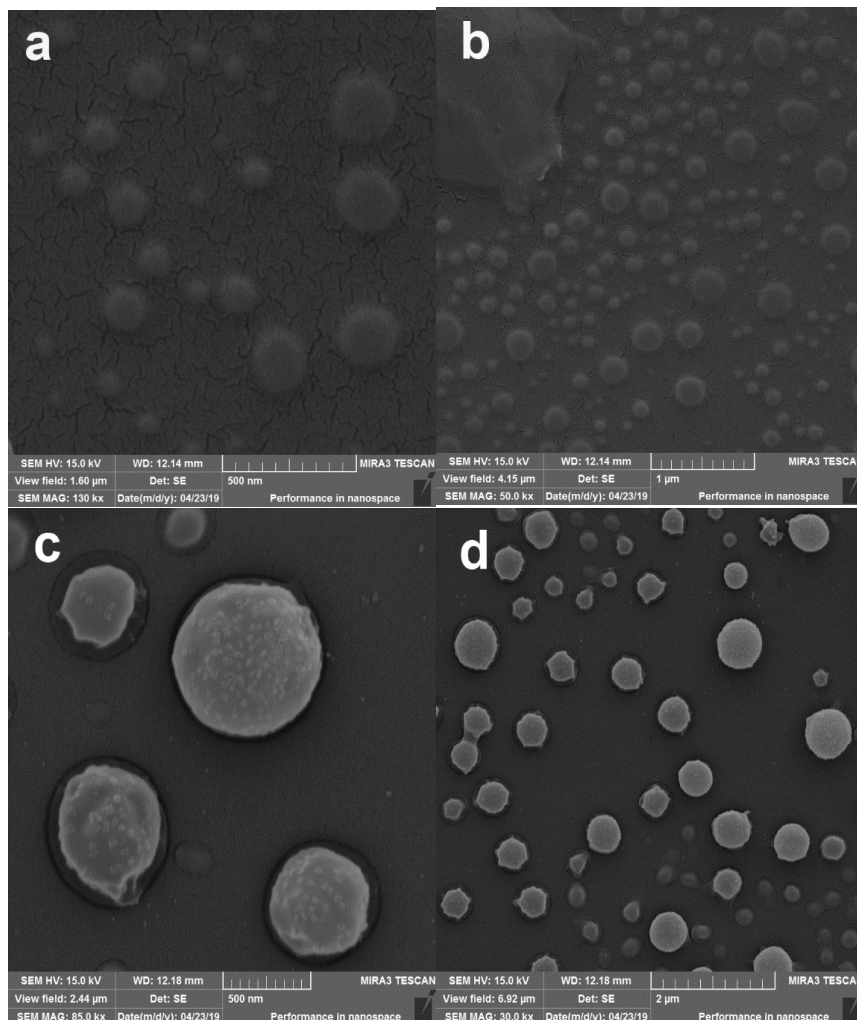Fig. 2 represent the SEM images of Si NPs (2a and 2b) and Si-g-PCA/Au (2c and 2d)

Fig. 2. SEM image of a, b) Si NPs and c, d) Si-g-PCA/Au.

nanocomposites. The polymeric shell of citric acid formed on the surface of the silica nanoparticles is illustrated in Fig. 2c. As shown in images 2c and 2d, gold nanoparticles are uniformly visible as sparkling spots, which are placed at the surface of the polymerized silica nanoparticles.

Fig. 3 shows the EDX map results for the Si-g-PCA/Au nanocomposite. The EDX maps show the presence of the silica, carbon, oxygen, and gold elements in the Si-g-PCA/Au nanocomposites with uniform dispersion and a significant percentage on the surface of polymerized Si nanoparticles. The results of the element analysis of EDX are shown in Fig. 4.

The BET surface area analysis technique was used to examine the surface properties of the Si-g-PCA/Au, such as surface area, total pore volume, pore radius, and pore size. The surface area is most often considered a critical property of any material, which can disclose imperative information about the adsorption properties. A higher surface area is desired chiefly over a lower
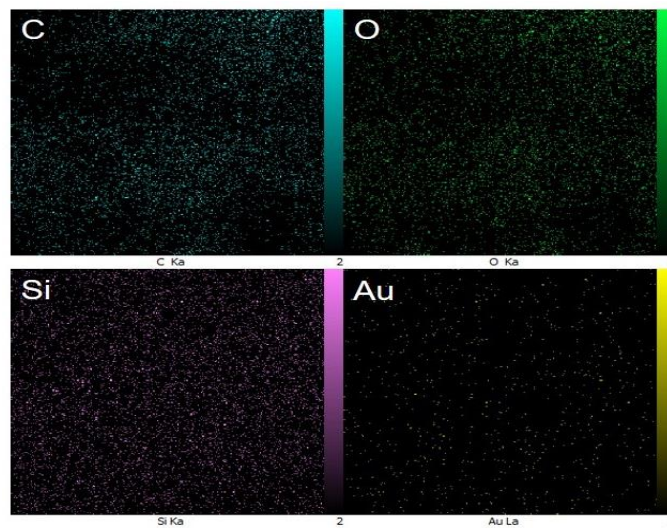

Fig. 3. EDX maps of the Si-g-PCA/Au nanocomposite.

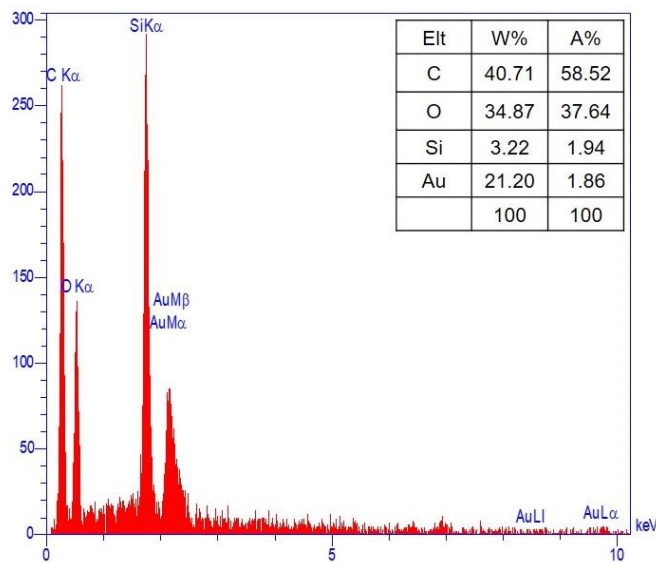| Elt	W%	A%
C	40.71	58.52
O	34.87	37.64
Si	3.22	1.94
Au	21.20	1.86
	100	100

Fig. 4. The results of the elemental analysis (EDX) of Si-g-PCA/Au nanocomposite.

one because it offers high sorption capacity. A higher number of small-sized pores has a high surface area in a controlled volume. As a result of nitrogen adsorption-desorption analysis, Si-g-PCA/Au samples showed a wide hysteresis loop at p/p_o= 0.02–0.99 (Fig. 5A) compared to a bimodal pore structure (Fig. 5B). The specific surface area (S_{BET}) value of the Si-g-PCA/Au was found to be 0.64011 m²/g by the N_2 isotherms (Fig. 5A) [38-40].

Spectral characteristics
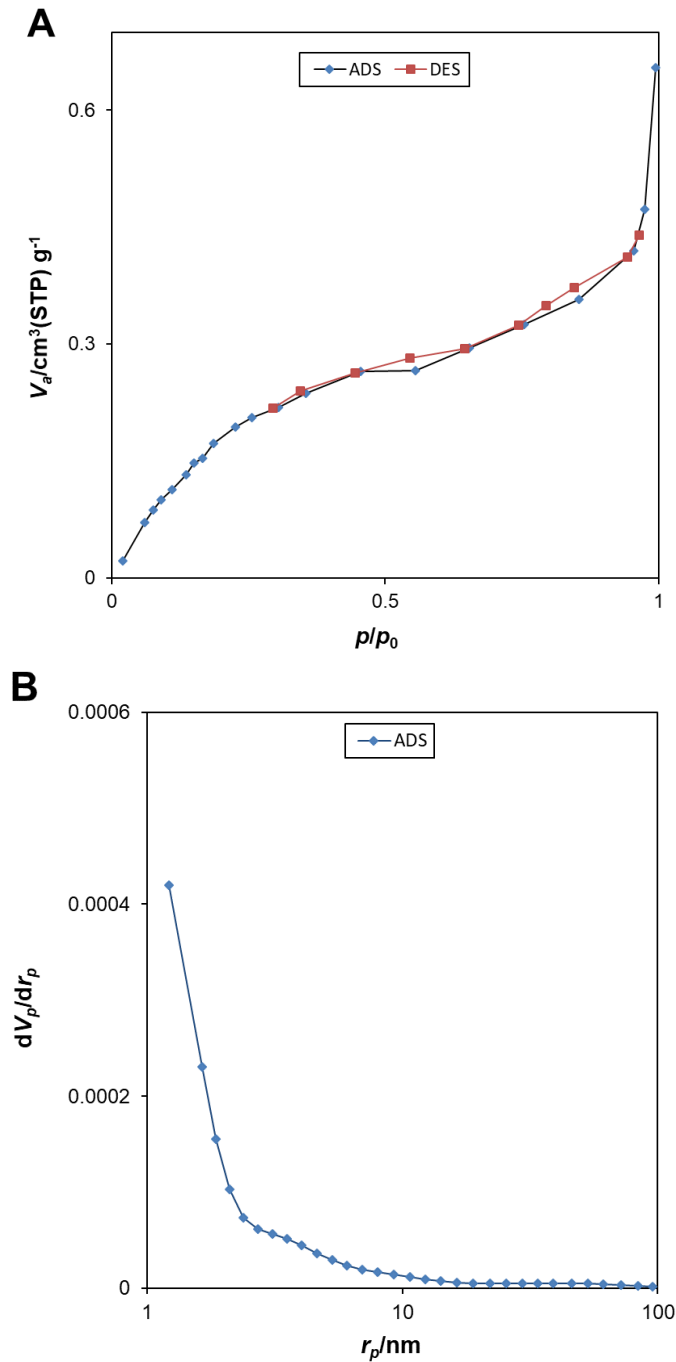
Fig. 6 (a, b) shows the ruby red color of the

Fig. 5. Nitrogen adsorption isotherms (A) and pore size distribution (B) of Si-g-PCA/Au nanocomposite.

Si-g-PCA/Au nanocomposite solution and its Uv-Vis spectra. Fig. 6c shows the Uv-Vis Spectra of gluten solution. In Fig. 6b, gold nanocomposites have a surface plasmon resonance peak at 530 nm [41], and the absorbance at 250 to 300 nm belongs to polymerized Si-g-PCA nanoparticles [36]. The absorbance peaks at the wavelengths of 230 and 280 nm in Fig. 6c belong to proteins in gluten solution. Proteins solution has a maximum absorbance at 200 and 280 nm. The absorbance peak at the wavelength of 230 nm belongs to transitions of $\pi \rightarrow \pi^*$ in the Peptide bonds and at 280 nm occurs because of amino acids with aromatic rings [42]. Excitation of the surface plasmon resonance in 530 nm and ruby red color of gold nanocomposites represent the successful synthesis of gold nanoparticles. The nanosensor has 3 absorption peaks at 280 to 400 nm, 500 to 600 nm, and 600 to 790. The sensor absorption of 530 nm with high intensity (Fig. 7a) shows the immobilization of the gold nanocomposites on the membrane. The smaller peak at about 700 nm belongs to gold nanoparticles, which agglomerated. As shown in Fig. 7b, the absorption of the nanosensor increases at all wavelengths

after exposure to the gluten solution. Fig. 8 shows nanosensor absorbance increases with increasing gluten concentration from 0.0 to 370.37 μgmL^{-1}. These absorption peaks show an increase in absorbance due to the increase in the gliadin concentration of gluten solution. The carboxylated silica NPs are suitable adsorbents for biomolecules such as proteins. Encapsulated gold NPs in polymeric shells of Si-g-PCA interacted with biomolecules such as proteins strongly. The adsorption is established through electrostatic interaction between the surface-terminated anionic groups $-COO^-$ on the nanoparticles and the positively charged amino groups $-NH_3^+$ of the gliadin of the gluten proteins. Apart from the electrostatic interaction, ionic/hydrogen bonding between $-NH_3^+$ and $-COO^-$ the functionalized surface is also possible [41]. The shape and the band maxima of absorption spectra of the nanosensor remain unchanged after reaction with gluten, and no other absorption band of the nanosensor towards the longer wavelength is noticed. This observation suggests that the interaction between nanosensor and gluten does not change the absorption and spectral properties. Also, any
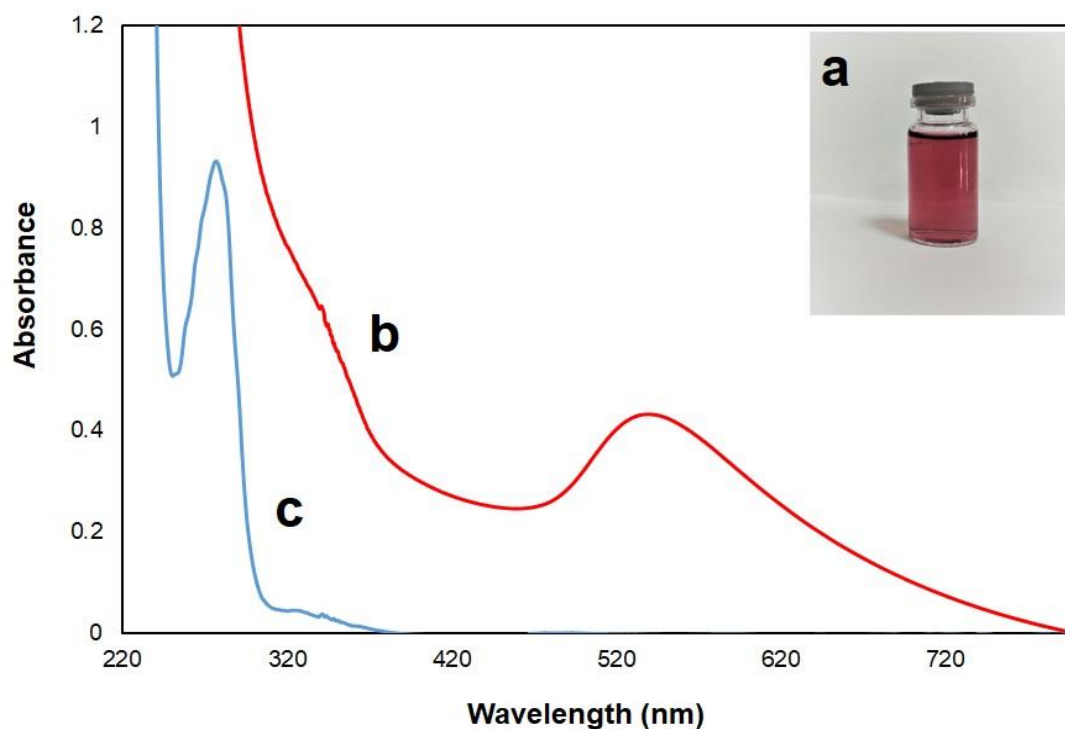

Fig. 6. a) Ruby red Si-g-PCA/Au nanocomposite solution, Uv-Vis spectra of b) Si-g-PCA/Au and c) gluten solution.
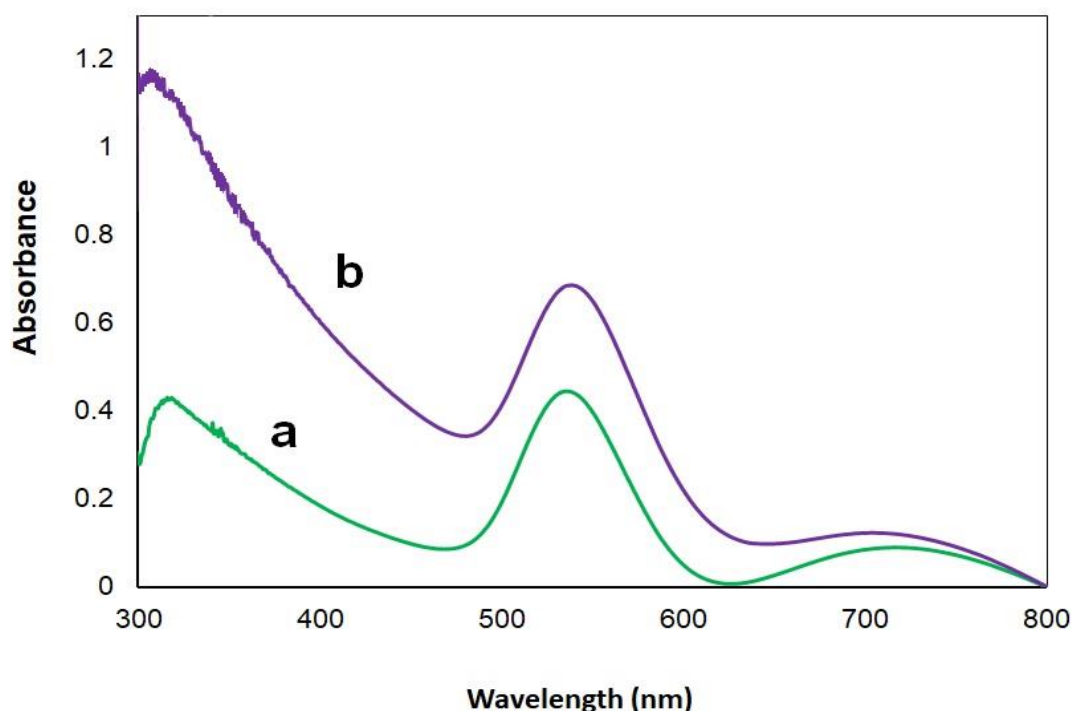
Fig. 7. The absorption spectrum of nanosensor a) before and b) after reaction with 215.31 µgmL^{-1} of gluten solution at pH 7.

chemical reaction may be discarded since no new absorption peak appears at a longer wavelength [43-46]. The conjugation of gliadin molecules to encapsulated gold nanoparticles into polymeric shell branches reduces the aggregation of gold nanoparticles and the bonding of plasmon surface bonds. Thus, the absorption of gold nanoparticles by protein conjugation was increased. Therefore, according to the given explanations, the increase in absorption in Fig. 8 is related to the increase in gluten concentration. So, all of the measurements were done at 530 nm.

SEM and AFM analysis

Fig. 9 (a, b, c) depicts the triacetyl cellulose membrane before (9a) and after (9b, c) interaction with Si-g-PCA/Au nanocomposites. As these figures show, the spherical nanocomposites have immobilized entirely and uniformly on the surface of the membrane.

Fig. 10 illustrates the SEM images of the nanosensor after reaction with gluten solution. These images clearly show the reaction between gliadin and nanosensor that has led to appear the star shape of the gliadin proteins on the surface of the nanosensor. Meanwhile, the spherical nanocomposites are still recognizable in the background. This issue confirms the reaction of the gold nanocomposites and gliadin proteins.

Surface imaging studies were done using atomic force microscopy (AFM) to evaluate surface morphology. Fig. 11 (a, b) shows the topographic images, (c) and (d) 3D topographic images, and (e) and (f) height profile of nanosensor before, and after exposure to gluten, respectively. The darker matrix in topographic images, Figs. 11a and 11c, depict polymerized silica nanoparticles and the bright spots depict encapsulated gold nanoparticles, which are recognizable on the surface of the nanosensor. Significant increases in the presence of peaks (Fig. 11f compress of Fig. 11e) and increase in the roughness (nm) of the nanosensor surface profile (Table 2) occur after the reaction with gluten. Ra, Rz and Rq are average surface roughness, the average square root of heights, and the average difference between the highest peak and the deepest hole, in Table 2.

Response Time

The important parameter that must be evaluated for each sensing phase is the response time of the fabricated nanosensor; which is controlled by the time required for the analyte
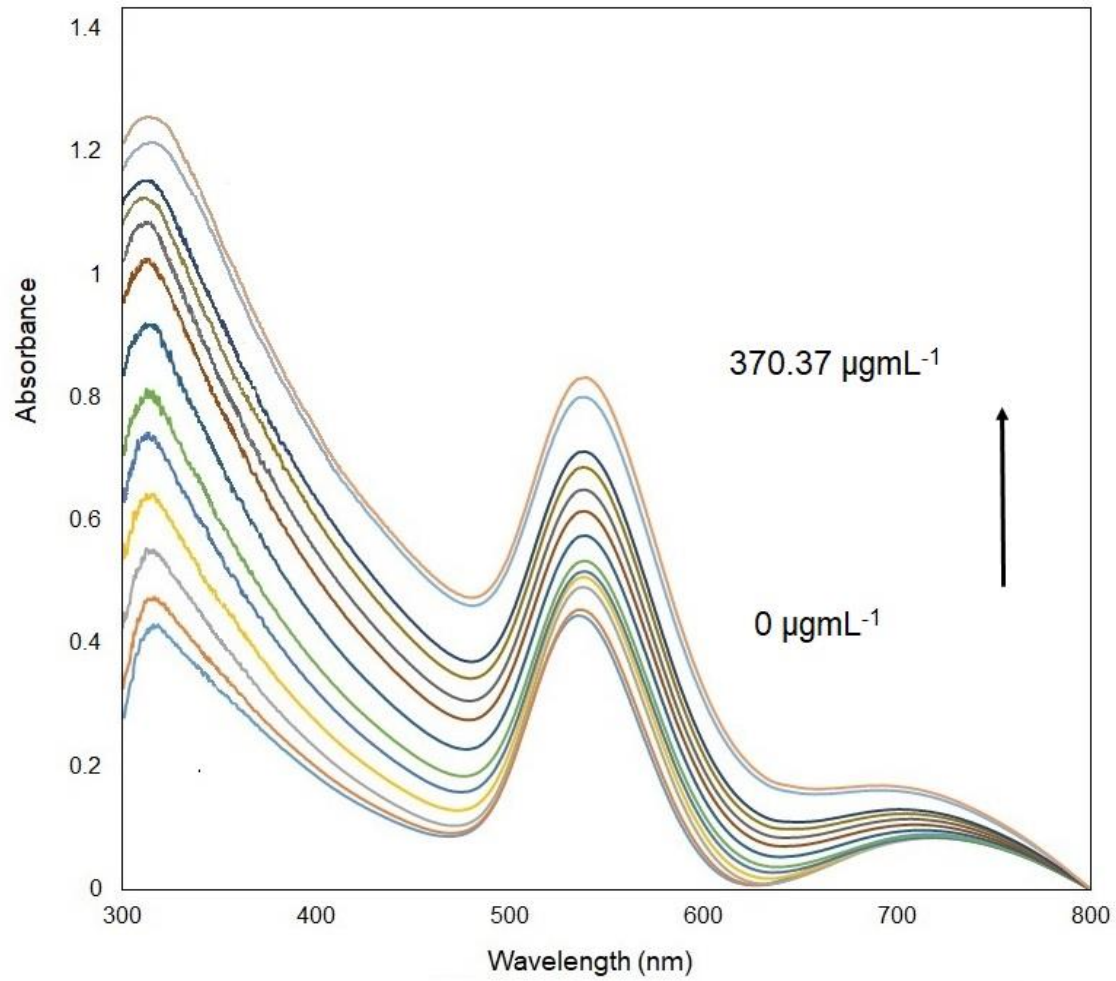
Fig. 8. The absorption spectrum of nanosensor in the presence of the different concentration of gluten solution: 0, 49.50, 73.89, 93.04, 145.63, 169.08, 192.31, 215.31, 238.09, 260.66, 283.02, 327.10, 348.84 and 370.37 μgmL^{-1} at pH 7.
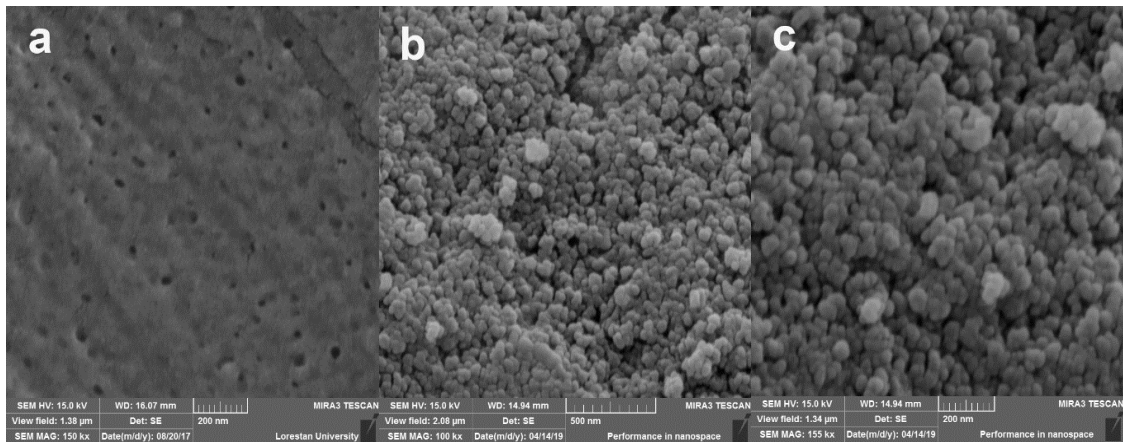

Fig. 9. SEM images of triacetyl cellulose membrane and b, c) membrane after coating with the Si-g-PCA/Au nanocomposite.
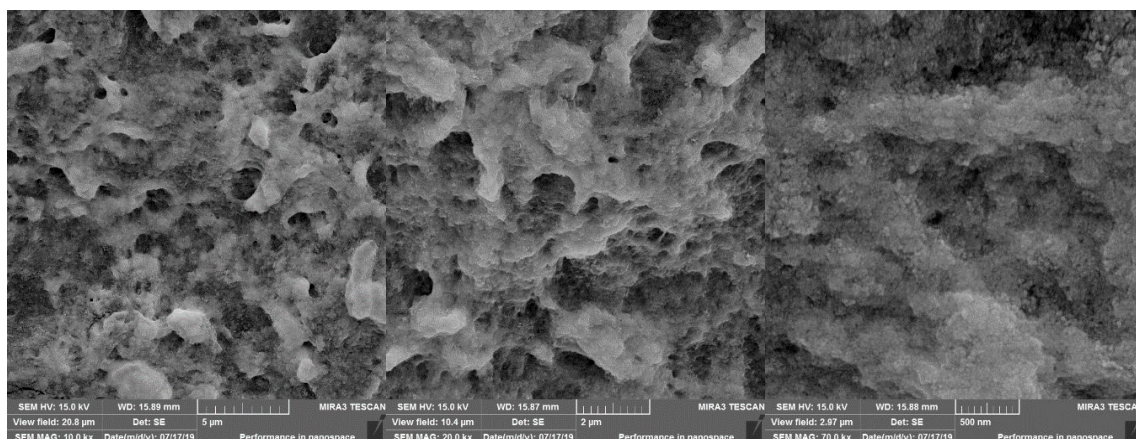
Fig. 10. SEM images of the nanosensor after reaction with gluten.

Table 2. The changes of nanosensor surface roughness (nm) before and after reaction with gluten.

Roughness (nm)	R_a	R_z	R_q
Before reaction	21.00	289.80	165.40
After reaction	25.66	345.20	205.30

Table 3. Analytical figures of merit for the proposed sensor.

Analyte	Dynamic range (μgmL^{-1})	Calibration Curve	LOD[*] (μgmL^{-1})	LOQ[*] (μgmL^{-1})	Response time (s)
Gluten	49.50–370.37	A=0.0011C + 0.4201 R^2=0.9918	12.14±0.03	40.58±0.06	60

[*]n=6

to diffuse from the bulk of the solution to the membrane interface and associate with the nanoreagent. For this purpose, the changes in the absorbance of the nanosensor were recorded versus time at 530 nm using selected experimental conditions for 121.95 and 260.1 μgmL^{-1} of gluten solutions. The obtained response curves for both concentrations of gluten are shown in Fig. 12. As can be seen, the absorbance increases until one minute and then remains constant. The membrane reached 95% of the final signal at 1 min. Therefore, 1 minute is considered as the response time of the nanosensor.

Analytical figures of merit

The calibration graph was obtained as a function of gluten concentration by plotting absorbance changes at 60 s. The absorbance measurements are expressed as the absorbance difference, defined as the difference between the absorbance of nanosensor in reaction solution in the absence and presence of gluten. As shown in Fig.13, the absorbance changes versus the gluten concentration plot exhibit a linear range over 49.50 to 370.37 μgmL^{-1} at pH 7 for a fixed time of 1 min. The regression equation is A=0.0011C + 0.4201 with a correlation coefficient of 0.9918, where C is the sample concentration in μgmL^{-1}. The limit of detection (LOD) and limit of quantification (LOQ) were calculated using three and ten times the standard deviation of the blank divided by the slope of the calibration curve was 12.14 and 40.58
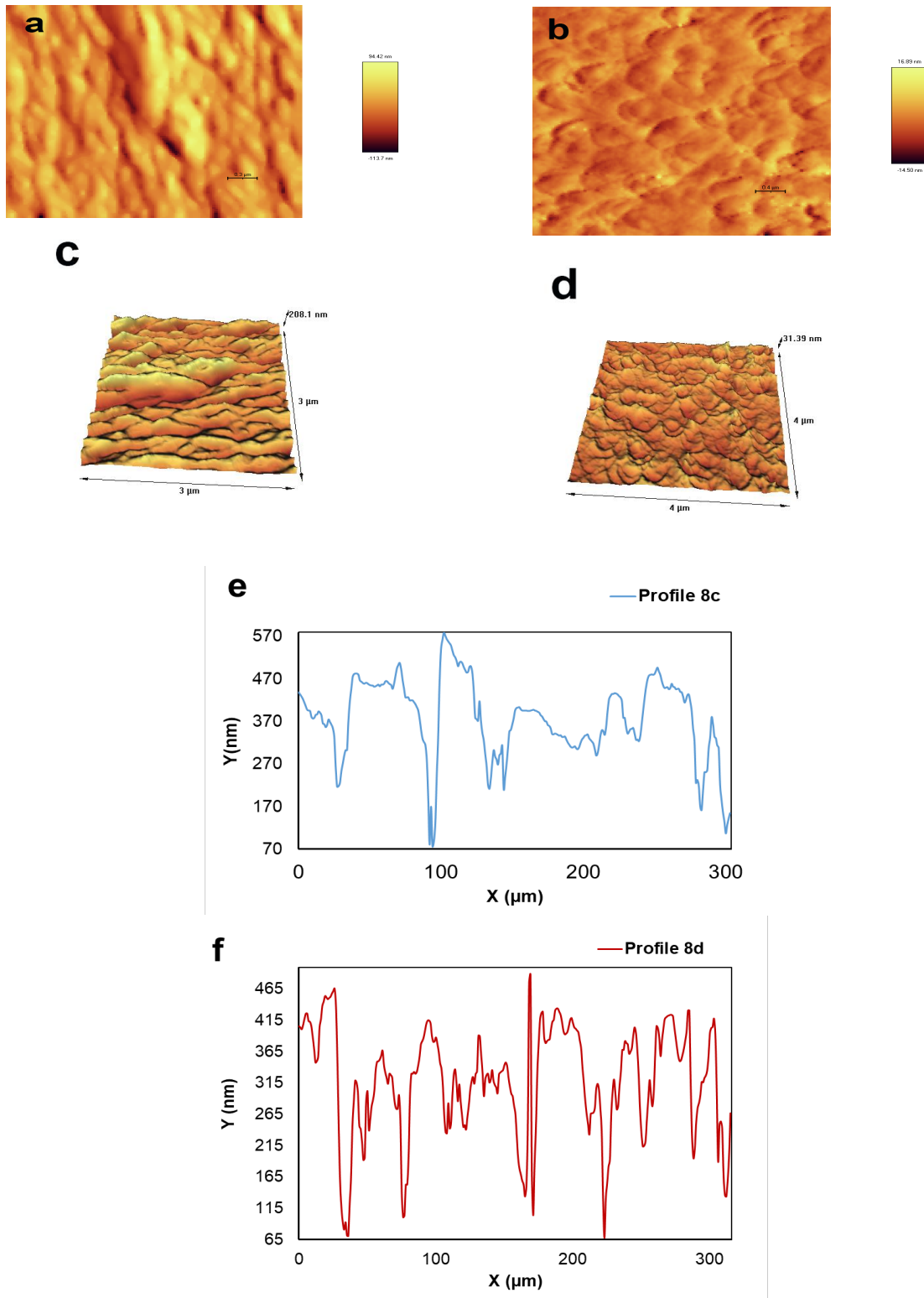
Fig. 11. The 2D and 3D topographic nanosensor AFM images, (a) and (c) before, (b) and (d) after reaction with gluten. (e) and (f) the corresponding height profiles images.
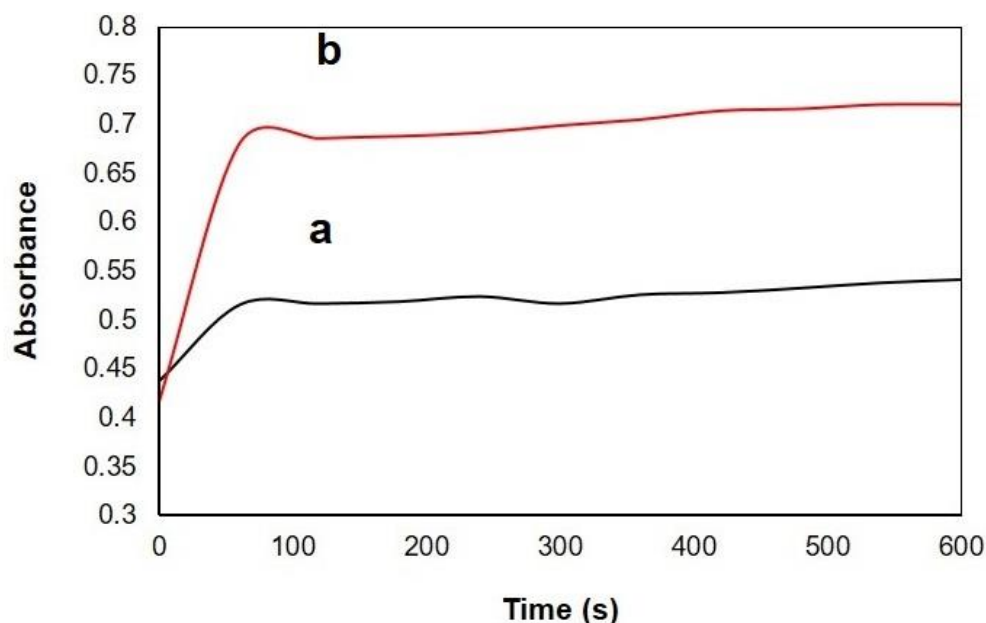
Fig. 12. Response time curve at 530 nm as a function of time in the presence of gluten with concentrations of (a) 121.95 and (b) 260.1 μgmL^{-1} at pH 7.

Table 4. Inter- and intra-day reproducibility of the nanosensor for determination of gluten.

Sample	RSD%[*]	
	Inter-day	Intra-day
Gluten (169.1 μgmL^{-1})	3.63	4.58

[*]n=5

μgmL^{-1} respectively. The analytical figures of merit for the determination of gluten are shown in Table 3.

Regeneration of the sensing phase

For confirmation of nanosensor reversibility, the used nanosensor was placed in a gluten solvent (55% ethanol) to investigate membrane regeneration. The sensing phase has a short regeneration time (1 min), and this process can be repeated 5 times. Gluten is reacted with the immobilized Si-g-PCA/Au on the surface of nanosensor. Then it was placed in gluten and regenerating solutions subsequently, and the on-use permanence of the sensing phase was obtained.

Reproducibility and reversibility

The nanosensor's reproducibility and reversibility in the determination of the gluten were checked out by repeatedly exposing the sensing phase to a gluten solution. The repeatability was evaluated by performing 5 determinations with the same standard gluten solution (Fig. 14). The inter-day and intra-day relative standard deviation (R.S.D.) for the response of one membrane towards a 169.1 μgmL^{-1} gluten solution was 3.63% and 4.58% respectively. Table 4 shows the results of the accuracy and precision of the gluten determination with this nanosensor. The results show that the reproducibility is satisfactory, and the nanosensor could be regenerated easily by
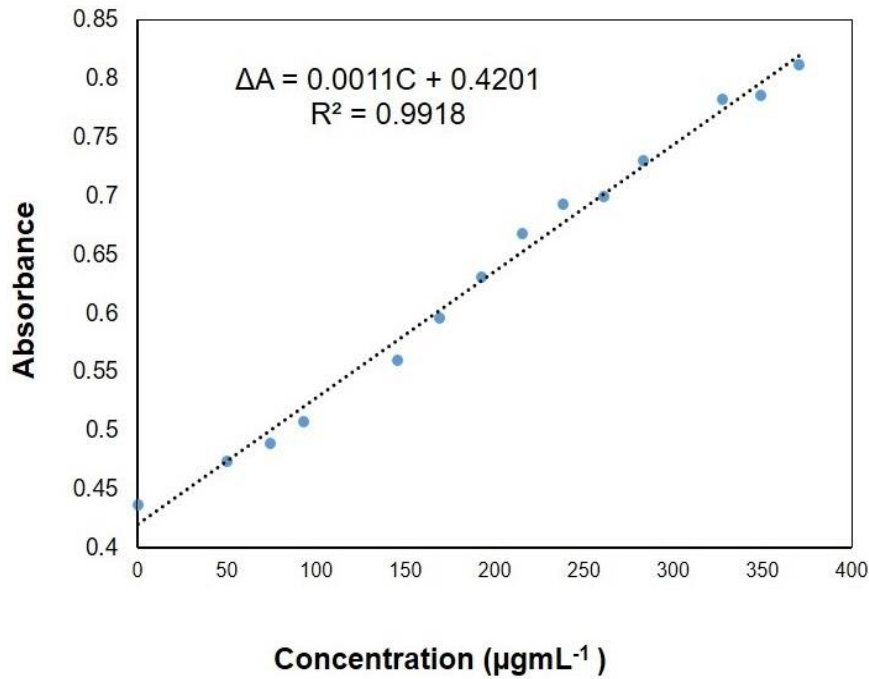
Fig. 13. Variation in absorbance for nanosensor as a function of gluten concentration.
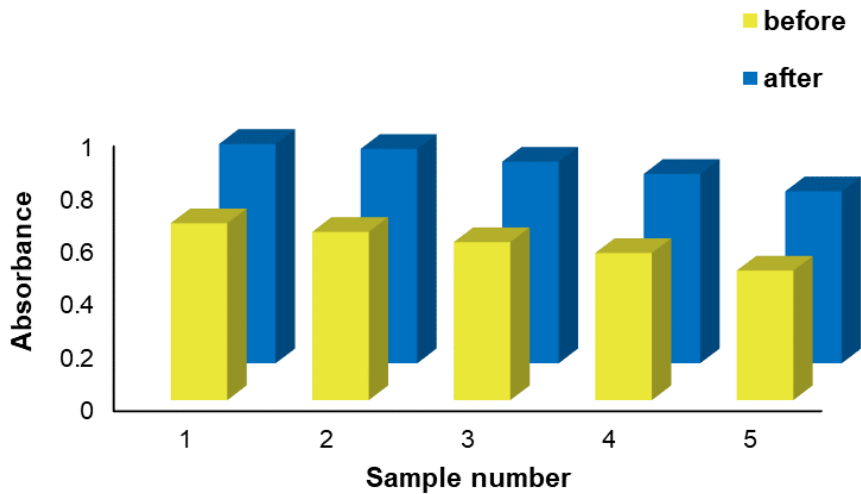

Fig. 14. Regeneration of sensing probe over five times in the presence of 169.1 μgmL^{-1} of gluten.

using a 55% ethanol solution.

Interference Study

The selectivity of the fabricated nanosensor was tested with several cations and anions as found chiefly in gluten extract solution such as Na^+, NH_4^+, Cl^-, K^+, PO_4^{3-}, NO_3^-, SO_4^{2-}, Citrate at concentrations up to 100 times of the analyte, in the presence of 145.63 μgmL^{-1} of gliadin and pH

7. Results are summarized in Table 5; the ions do not interfere with gluten measuring. The resulting relative error is defined as RE (%) = $[(A_2 - A_1)/A_1] \times 100$ (absorbance before (A_1) and after (A_2) addition of potentially interfering ions).

Real Sample analysis

The analytical efficiency of the developed nanosensor was evaluated in real sample analysis,

Table 5. Influence of interfering species on the determination of 145.63 μgmL^{-1} gluten.

Interference	Absorbance change $\Delta A = A_2 - A_1$	Relative error RE (%) = $(A_2 - A_1)/A_1] \times 100$
Na^+	0.00745	1.35
NH_4^+	0.00818	1.48
Cl^-	0.00266	0.484
K^+	0.00701	1.27
PO_4^{3-}	0.00381	0.693
NO_3^-	0.00569	1.03
SO_4^{2-}	0.00363	0.66
citrare	0.00272	0.49

Table 6. Determination of gluten in real samples at the optimum conditions.

Sample	Added (μgmL^{-1})	Measured (μgmL^{-1})*	Recovery %*
"Celino Kalleh" gluten free white toast bread	0 73.1 145.6	<LOD 72.43±0.31 147.71±0.45	... 99.1 % 101.45 %
"Celino kalleh" gluten free lavash bread	0 73.1 145.6	<LOD 73.34±0.64 149.59±0.35	... 100.34 % 102.74 %

* n=3

and two glutens-free bread from "Kaleh Company" were tested. One of the complicated issues in the food industry is the extraction of heat-treated gluten from food that has developed based on several extraction solutions in recent years. In the most of these protocols, the food sample is first treated with 0.5 M NaCl to remove albumins and globulins and then use alcohol-water solutions to extract the gluten [47, 48]. As mentioned before, gluten extraction was accomplished with wheat gluten powder that its fat, starch, and metabolic proteins have been removed after treatment with dimethyl chloride and NaCl solution. Gluten proteins was extracted with ethanol-water 55% and glutenins were separated by phase separation at low temperatures. Therefore, it is expected that only the remaining metabolite in the solution to be gliadin. [37]. The standard addition recovery method apply for fabricated nanosensor assessment. A standard solution with a certain

amount of gluten (73.1 and 145.6 μgmL^{-1}) was added to real samples, and the measurements were repeated 3 times. The results are shown the excellent reliability and reproducibility of the method for determining the gluten in flour solutions (Table 6).

CONCLUSION

This work investigates the nature of the interaction between Si-g-PCA/Au nanosensor and gluten. Si-g-PCA/Au nanocomposite was synthesized using sonochemical method, first silica NPs polymerized with Poly citric acid and then Au NPs encapsulated in polymeric shell. In the next step, this nanocomposite was immobilized on triacetyl cellulose membrane to fabricate an optical nanosensor. Gluten proteins enormously increase the absorbance of the sensing phase. The experimental results indicate that the probable reaction mechanism of nanosensor with gluten

is electrostatic interaction. The unchanged shape and the band maxima of absorption spectra of the nanosensor without appearing a new absorption peak after reaction with the gluten suggest that the interaction between the nanosensor and gluten does not change the absorption and spectral properties or any chemical reaction between them. The as-prepared sensor showed an increment at 530 nm in the presence of various concentrations of gluten. The nanosensor had a linear range from 49.50 to 370.37 μgmL^{-1} for gluten determination, with LOD and LOQ 12.14 and 40.58 μgmL^{-1}, respectively. The present sensor determined the gluten in gluten-free real samples quickly. Furthermore, the sensor showed that it can be recovered in the presence of 55% ethanol and has a multi-usage capability. The proposed sensor has a long lifetime and faster response time than previously reported sensors for gluten determination. This nanosensor is easy to use and requires no special skills or instruments.

ACKNOWLEDGEMENT

CONFLICT OF INTEREST

The authors declare that there is no conflict of interests regarding the publication of this manuscript.

REFERENCES

1. Loussert C, Popineau Y, Mangavel C. Protein bodies ontogeny and localization of prolamin components in the developing endosperm of wheat caryopses. Journal of Cereal Science. 2008;47(3):445-456.
2. Varriale A, Rossi M, Staiano M, Terpetschnig E, Barbieri B, Rossi M, et al. Fluorescence Correlation Spectroscopy Assay for Gliadin in Food. Anal Chem. 2007;79(12):4687-4689.
3. Leszczyńska J, Łącka A, Bryszewska M, Brzezińska-Błaszczyk E. The usefulness of rabbit anti-QQQPP peptide antibodies to wheat flour antigenicity studies. Czech Journal of Food Sciences. 2008;26(No. 1):24-30.
4. Orth RA, Baker RJ, Bushuk W. STATISTICAL EVALUATION OF TECHNIQUES FOR PREDICTING BAKING QUALITY OF WHEAT CULTIVARS. Canadian Journal of Plant Science. 1972;52(2):139-146.
5. Wieser H. Chemistry of gluten proteins. Food Microbiol. 2007;24(2):115-119.
6. O'Brien S, Wang Y-J. Susceptibility of annealed starches to hydrolysis by α-amylase and glucoamylase. Carbohydr Polym. 2008;72(4):597-607.
7. Masson-Matthee MD. The Codex Alimentarius: Harmonisation Through Standard-Setting. The Codex Alimentarius Commission and Its Standards: T.M.C. Asser Press; 2007. p. 51-94.
8. Fasano A, Catassi C. Celiac Disease. New England Journal of Medicine. 2012;367(25):2419-2426.
9. Collin P, Vilska S, Heinonen PK, Hallstrom O, Pikkarainen P. Infertility and coeliac disease. Gut. 1996;39(3):382-384.
10. Shan L, Molberg Ø, Parrot I, Hausch F, Filiz F, Gray GM, et al. Structural Basis for Gluten Intolerance in Celiac Sprue. Science. 2002;297(5590):2275-2279.
11. Bogue R. Nanosensors: a review of recent research. Sensor Review. 2009;29(4):310-315.
12. Sekhon B. Nanotechnology in agri-food production: an overview. Nanotechnology, Science and Applications. 2014:31.
13. Bietz JA, Burnouf T. Chromosomal control of wheat gliadin: analysis by reversed-phase high-performance liquid chromatography. Theor Appl Genet. 1985;70(6):599-609.
14. Scanlon MG, Bushuk W. Application of photodiode-array detection in RP-HPLC of gliadins for automated wheat variety identification. Journal of Cereal Science. 1990;12(3):229-234.
15. Larre C, Popineau Y, Loisel W. Fractionation of gliadins from common wheat by cation exchange FPLC. Journal of Cereal Science. 1991;14(3):231-241.
16. Dworschak RG, Ens W, Standing KG, Preston KR, Marchylo BA, Nightingale MJ, et al. Analysis of wheat gluten proteins by matrix-assisted laser desorption/ionization mass spectrometry. J Mass Spectrom. 1998;33(5):429-435.
17. Woychik JH, Boundy JA, Dimler RJ. Starch gel electrophoresis of wheat gluten proteins with concentrated urea. Archives of Biochemistry and Biophysics. 1961;94(3):477-482.
18. Kasarda DD, Bernardin JE, Qualset CO. Relationship of gliadin protein components to chromosomes in hexaploid wheats (Triticum aestivum L.). Proceedings of the National Academy of Sciences. 1976;73(10):3646-3650.
19. Shewry PR, Faulks AJ, Pratt HM, Miflin BJ. The varietal identification of single seeds of wheat by sodium dodecyl-sulphate polyacrylamide gel electrophoresis of gliadin. Journal of the Science of Food and Agriculture. 1978;29(10):847-849.
20. Zillman RR, Bushuk W. WHEAT CULTIVAR IDENTIFICATION BY GLIADIN ELECTROPHOREGRAMS. III. CATALOGUE OF ELECTROPHOREGRAM FORMULAS OF CANADIAN WHEAT CULTIVARS. Canadian Journal of Plant Science. 1979;59(2):287-298.
21. Du Cros DL, Wrigley CW. Improved electrophoretic methods for identifying cereal varieties. Journal of the Science of Food and Agriculture. 1979;30(8):785-794.
22. Wilson DL. Two-Dimensional Polyacrylamide Gel Electrophoresis of Proteins. Experimental Neurochemistry: Springer US; 1982. p. 133-146.
23. Wrigley CW. Protein mapping by combined gel electrofocusing and electrophoresis: Application to the study of genotypic variations in wheat gliadins. Biochem Genet. 1970;4(4):509-516.
24. Mecham DK, Kasarda DD, Qualset CO. Genetic aspects of wheat gliadin proteins. Biochem Genet. 1978;16(7-8):831-853.
25. Jackson EA, Holt LM, Payne PI. Glu-B2, a storage protein locus controlling the D group of LMW glutenin subunits in bread wheat (Triticum aestivum). Genet Res. 1985;46(1):11-17.
26. Sandberg M, Lundberg L, Ferm M, Malmheden Yman I.

Real Time PCR for the detection and discrimination of cereal contamination in gluten free foods. European Food Research and Technology. 2003;217(4):344-349.

27. López-López L, Miranda-Castro R, de-los-Santos-Álvarez N, Miranda-Ordieres AJ, Lobo-Castañón MJ. Disposable electrochemical aptasensor for gluten determination in food. Sensors Actuators B: Chem. 2017;241:522-527.

28. Weng X, Gaur G, Neethirajan S. Rapid Detection of Food Allergens by Microfluidics ELISA-Based Optical Sensor. Biosensors. 2016;6(2):24.

29. Ontiveros G, Hernandez P, Ibarra IS, Dominguez JM, Rodriguez JA. Development of a Biosensor Modified with Nanoparticles for Sensitive Detection of Gluten by Chronoamperometry. ECS Transactions. 2017;76(1):103-107.

30. Chu P-T, Lin C-S, Chen W-J, Chen C-F, Wen H-W. Detection of Gliadin in Foods Using a Quartz Crystal Microbalance Biosensor That Incorporates Gold Nanoparticles. Journal of Agricultural and Food Chemistry. 2012;60(26):6483-6492.

31. Martín-Fernández B, de-los-Santos-Álvarez N, Martín-Clemente JP, Lobo-Castañón MJ, López-Ruiz B. Challenging genosensors in food samples: The case of gluten determination in highly processed samples. Talanta. 2016;146:490-495.

32. García-García A, Madrid R, Sohrabi H, de la Cruz S, García T, Martín R, et al. A sensitive and specific real-time PCR targeting DNA from wheat, barley and rye to track gluten contamination in marketed foods. LWT. 2019;114:108378.

33. Iskierko Z, Sharma PS, Noworyta KR, Borowicz P, Cieplak M, Kutner W, et al. Selective PQQPFPQQ Gluten Epitope Chemical Sensor with a Molecularly Imprinted Polymer Recognition Unit and an Extended-Gate Field-Effect Transistor Transduction Unit. Anal Chem. 2019;91(7):4537-4543.

34. Karst U. Chemical and biochemical sensors. Edited by W. Göpel, T. A. Jones, M. Kleitz, I. Lundström and T. Seiyama, Volumes 2 and 3 of Sensors?A Comprehensive Survey, edited by W. Göpel, J. Hesse and J. N. Zemel, VCH Weinheim 1991, 716 pp., hardcover, DM 380, ISBN 3-527-26768-9 (Vol. 2); 514 pp., hardcover, DM 380, ISBN 3-527-26769-7 (Vol. 3). Adv Mater. 1993;5(1):64-65.

35. Afkhami A, Sarlak N. Design and characteristics of a sulfide and sulfite optode based on immobilization of methyl violet on a triacetylcellulose membrane. Sensors Actuators B: Chem. 2007;124(2):285-289.

36. Sarlak N, Meyer TJ. Fabrication of completely water soluble graphene oxides graft poly citric acid using different oxidation methods and comparison of them. J Mol Liq. 2017;243:654-663.

37. Boire A, Menut P, Morel M-H, Sanchez C. Phase behaviour of a wheat protein isolate. Soft Matter. 2013;9(47):11417.

38. Roosta M, Ghaedi M, Shokri N, Daneshfar A, Sahraei R, Asghari A. Optimization of the combined ultrasonic assisted/adsorption method for the removal of malachite green by gold nanoparticles loaded on activated carbon: Experimental design. Spectrochimica Acta Part A: Molecular and Biomolecular Spectroscopy. 2014;118:55-65.

39. Kamel RM, Shahat A, Anwar ZM, El-Kady HA, Kilany EM. Efficient dual sensor of alternate nanomaterials for sensitive and rapid monitoring of ultra-trace phenols in sea water. J Mol Liq. 2020;297:111798.

40. Kamel RM, Mohamed SK. Highly sensitive solid-state fluorescent sensor immobilized on silica nanoparticles for direct detection dimethyl phenol in seawater samples. J Mol Struct. 2021;1246:131128.

41. Wangoo N, Suri CR, Shekhawat G. Interaction of gold nanoparticles with protein: A spectroscopic study to monitor protein conformational changes. Appl Phys Lett. 2008;92(13):133104.

42. Aitken A, Learmonth M. Protein Determination by UV Absorption. Springer Protocols Handbooks: Humana Press; 1996. p. 3-6.

43. Azab HA, Kamel RM. Binding of chlorfenvinphos and malathion with DNA and their detection using new sensitive luminescent Tb(III) complex probe. J Lumin. 2016;170:671-678.

44. Kamel RM, Mohamed SK, Mahmoud MA. High-throughput sensor microtiter plate of new terbium complexes for the determination of anthracene in seawater. Spectrochimica Acta Part A: Molecular and Biomolecular Spectroscopy. 2022;266:120474.

45. Kamel RM, El-Sakka SS, Bahgat K, Monir MR, Soliman MHA. New turn on fluorimetric sensor for direct detection of ultra-trace ferric ions in industrial wastewater and its application by test strips. J Photochem Photobiol A: Chem. 2021;411:113218.

46. Abbas AM, Anwar ZM, Soliman YA, Abdel-Hadi MM, Kamel RM. A turn-off luminescent europium probe for efficient and sensitive detection of some low molecular weight polycyclic aromatic hydrocarbons in seawater. Microchem J. 2020;159:105471.

47. van Eckert R, Berghofer E, Ciclitira PJ, Chirdo F, Denery-Papini S, Ellis HJ, et al. Towards a new gliadin reference material–isolation and characterisation. Journal of Cereal Science. 2006;43(3):331-341.

48. Chu P-T, Wen H-W. Sensitive detection and quantification of gliadin contamination in gluten-free food with immunomagnetic beads based liposomal fluorescence immunoassay. Anal Chim Acta. 2013;787:246-253.